VENUS GRAVITY

Grant NAGW-2361

Final Report
For the period 1 February 1991 through 31 January 1993

Semiannual Status Report Nos. 1, 2 and 3
For the period 1 February 1991 through 31 January 1993

Principal Investigator
Robert D. Reasenberg

June 1993

Prepared for
National Aeronautics and Space Administration
Washington, DC 20546

Smithsonian Institution
Astrophysical Observatory
Cambridge, MA 02138

The Smithsonian Astrophysical Observatory
is a member of the
Harvard-Smithsonian Center for Astrophysics

The NASA Technical Officer for this grant is Dr. Joseph M. Boyce, Code SL, Solar System Exploration Division, NASA Headquarters, Washington, DC 20546.

Venus Gravity Study Final Report

This is a final report and the July 1991 semiannual report of the work done under NASA Grant NAGW-2361 for the preparation and publication of a report on the previous work that yielded a model of the gravity field of Venus based on the Doppler tracking data from the Pioneer Venus Orbiter. The grant for $5,960 was in response to our letter proposal P2340-11-90 of 21 November 1990.

A paper describing our model of the gravity of Venus has appeared in JGR (Planets), copy appended. In order to make our work more useful to the community, we provided our digital map to the NSSDC, as indicated in the last paragraph of the paper.

The paper in JGR appears to have been well received. In March 1993, I received a request from Dr. Peter Cattermole, FRAS, for permission to include the color maps of Venus gravity and smoothed topography in a forthcoming book, VENUS -- THE NEW GEOLOGY, University College London Press. I have agreed to his request and sent him all necessary materials.

JOURNAL OF GEOPHYSICAL RESEARCH, VOL. 97, NO. E9, PAGES 14,681–14,690, SEPTEMBER 25, 1992

High-Resolution Gravity Model of Venus

R. D. REASENBERG AND Z. M. GOLDBERG

Radio and Geoastronomy Division, Smithsonian Astrophysical Observatory, Harvard-Smithsonian Center for Astrophysics, Cambridge, Massachusetts

The anomalous gravity field of Venus shows high correlation with surface features revealed by radar. We extract gravity models from the Doppler tracking data from the Pioneer Venus Orbiter (PVO) by means of a two-step process. In the first step, we solve the nonlinear spacecraft state estimation problem using a Kalman filter-smoother. The Kalman filter has been evaluated through simulations. This evaluation and some unusual features of the filter are discussed. In the second step, we perform a geophysical inversion using a linear Bayesian estimator. To allow an unbiased comparison between gravity and topography, we use a simulation technique to smooth and distort the radar topographic data so as to yield maps having the same characteristics as our gravity maps. The maps presented cover 2/3 of the surface of Venus and display the strong topography-gravity correlation previously reported. The topography-gravity scatter plots show two distinct trends.

1. INTRODUCTION

The Doppler tracking data from the Pioneer Venus Orbiter (PVO) contain the signature of the only available direct probe of the planet's internal structure: gravity. Illuminating that internal structure is the prime objective of our study of Venus gravity. Early investigations of the gravity field of Venus were based on the analyses of tracking data from fly-by missions [*Anderson and Efron*, 1969; *Howard et al.*, 1974; *Akim et al.*, 1978]. With the possible exception of the planetary mass estimate, these studies are superseded by the analyses of PVO data. In addition to the studies of local features by *Phillips et al.* [1979], *Sjogren et al.* [1980, 1983, 1984], *Reasenberg et al.* [1981, 1982], and *Goldberg and Reasenberg* [1985], there have been evaluations of the low-order spherical harmonic components of the field by *Ananda et al.* [1980], *Williams et al.* [1983], and *Mottinger et al.* [1985] and a determination of an eighteenth degree and order spherical harmonic model by *Bills et al.* [1987]. The gravity model presented here provides the highest resolution yet available, and the companion topography model, which mimics the resolution of the gravity model, provides a convenient means of forming and checking geophysical hypotheses.

For an overview of the PVO mission, see *Colin* [1980]; for a further description of the scientific results, see the references and bibliography therein and the other papers in the same issue of the *Journal of Geophysical Research*. More recent results are given by *Hunten et al.* [1983].

Our analysis is based on a two-stage procedure. In the first stage, we use a Kalman-Bucy filter-smoother to solve the nonlinear spacecraft state estimation problem. The filter is incorporated in the Planetary Ephemeris Program (PEP) [*Ash*, 1972]. Significant attributes of this filter are described in section 4. The results of some studies of the filter's performance are presented in section 5. Our analysis of the Venus gravity data is the first successful use of a Kalman filter as a tool for determining a planetary gravity field.

The geophysical inversion performed in the second stage is described by *Goldberg and Reasenberg* [1985], who also briefly discuss the Kalman-Bucy filtering. The inversion is carried out in a series of overlapping patches, each covering about 50° of longitude and extending as far poleward as the data allow. The overlap is sufficient to yield a band of at least 10° longitudinal width in which there is no significant difference in the models. Outside of that band, edge effects are noticeable, and the solutions there are discarded. The successive patches are merged smoothly within the band of agreement. The motivation for this approach is found in section 3 following a general discussion of the problem of planetary gravity and the information flow in our analysis, which are presented in section 2.

Paper number 92JE01499.

2. VENUS GRAVITY AND TOPOGRAPHY

Figure 1 shows the natural flow of information from internal geophysical processes to our Doppler observable. Those internal processes, acting within the bulk of the planet and driven by the escape of heat, give rise to its mass distribution, which is partially manifested as topography. The mass distribution, including the topography, produces the external gravity field. Given the initial position and velocity of a spacecraft, its subsequent motion is determined by the Venus gravity field along with perturbations from the Sun and other planets. The phase-coherent radio tracking system used by the NASA Deep Space Network yields a Doppler shift observable which reflects the spacecraft motion.

Ideally, we would like to invert all of these processes. Starting with the spacecraft observable, we would like to know the internal processes within the planet Venus. By well-established techniques, one can use the Doppler observable to determine the spacecraft motion. Similarly, to within resolution limits imposed by the data, the observing geometry, and the noise, that same observable can be used to determine directly the external gravitational field. On the other hand, the internal mass distribution cannot, in principle, be determined from the external gravitational field even if the latter were perfectly known. The problem of determining the internal processes responsible for the mass distribution is not even well defined. It comprises a major portion of the study of planetary interiors.

To shed some light on those internal processes and their resulting mass distributions, we can construct models. For

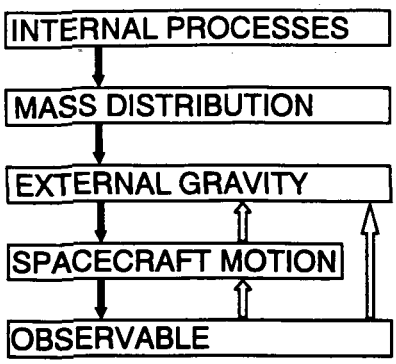

Fig. 1. The flow of information (causality) from internal processes, which are driven by the temperature difference between the surface and the interior, to the spacecraft Doppler observable. Open arrows show mathematically possible inversions.

those models applicable in the near-surface region, the observable consequences will include both the topography and the external gravitational field. For some types of internal processes, it is possible to obtain a relationship between the observed topography and the corresponding gravity anomalies. Such a signature can then be sought in the data. However, for Venus the resolution and fidelity of the gravity model are poor compared to that of the topography. Thus a direct comparison between the two would suffer a wavelength-dependent bias which would systematically distort any conclusions about the internal structure.

To overcome this problem of bias, we need a topographic map having the same distortion and spectral characteristics as the gravity model. Figure 2 is a simplified diagram of the information flow within our data processing system. In order to produce the required smoothed topography map, we start with the topographic data and calculate the corresponding spacecraft acceleration along the actual spacecraft trajectory, assuming the topography to be uncompensated and of unit density. These accelerations are processed by our linear inverter in the same way as the spacecraft Doppler rate residuals, yielding, respectively, the smoothed topography and gravity models. As shown by *Goldberg and Reasenberg* [1985], the resulting gravity model is of high fidelity; its location-dependent resolution and limited distortions are both well mimicked by the corresponding smoothed topography.

3. Pioneer Venus and the Analysis Problem

The orbital characteristics of PVO are the dominant factor in determining the resolution of our gravity maps and in selecting the analysis techniques. During the first 600 days of the mission, the altitude of the PVO at periapsis was maintained between approximately 140 and 190 km by means of propulsive maneuvers. The characteristics of the gravity maps that can be derived from the PVO tracking data are delimited by this low periapsis altitude, the high orbital eccentricity $e = 0.84$, an orbital inclination of 105° to the Venus equator, and the evolving Venus-Earth-Sun geometry, which includes superior conjunctions and occultations by Venus of the spacecraft near periapsis. In particular, the PVO Doppler data support high-resolution maps in the vicinity of the spacecraft periapsis, whose latitude remained between 17° and 14°N during the first 600 days. However, at 45° along track from periapsis, where the spacecraft local altitude was about 1100 km, the possible resolution of the maps is correspondingly lower. Data used in our analysis were obtained when the Earth-Venus-spacecraft angle at periapsis was less than 90° and when the Earth-Sun-Venus angle was less than 150°.

Two sets of circumstances together set the framework for selecting the analysis technique. The first pertains to the way the spacecraft moved, and the second pertains to where it moved with respect to the surface of Venus. These are addressed in order. The deterministic trajectories of celestial mechanics are an excellent representation of the motions of most planets and natural satellites on a time scale of recorded history. These classical models justifiably neglect such stochastic perturbations as the variation in solar radiation pressure due to albedo variations. However, spacecraft are different; they have about an eight-order larger area-to-mass ratio and may contain outgassing components (e.g., in the attitude control system) that produce accelerations significant to the analysis of tracking data. Such stochastic contributions to the driving terms of a model of a system are known generally as "process noise" and are dealt with by means of the Kalman-Bucy filter. (For a discussion of such filters, see, for example, *Jazwinski* [1970] and *Gelb* [1974].)

The spacecraft acceleration along the line of sight is measured by the Doppler rate data obtained by (numerical) differentiation of the Doppler tracking data. To be of use in a geophysical analysis, this measure must be "downward continued" to the surface and transformed into a uniform representation. The surface resolution of such an inversion is limited to being not much better than $\lambda = 2\pi h$, where λ is the spatial wavelength on the surface and h is the local spacecraft altitude. For a surface mass density (represented as a surface harmonic series) the external vertical acceleration is

$$a = -\frac{\partial V}{\partial r} = \sum_{n=2}^{\infty} (n+1) \frac{r_0^{n+1}}{r^{n+2}} \sum_{m=0}^{n} P_{nm}(\cos\theta) \cdot [c_{nm} \cos(m\varphi) + S_{nm} \sin(m\varphi)] \quad (1)$$

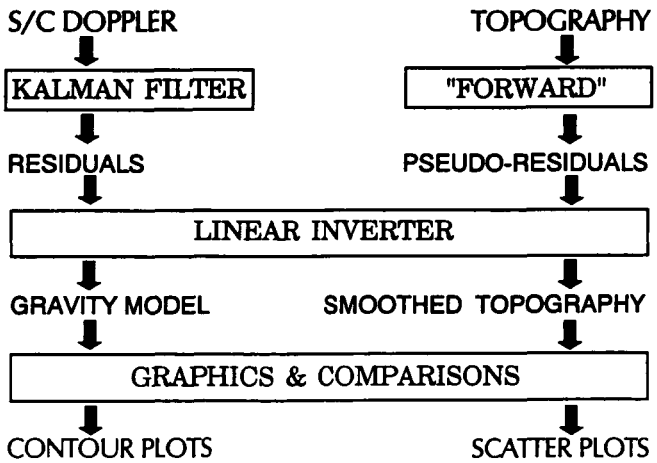

Fig. 2. The flow of information within our data processing system. The processors (computer programs) are in the boxes. The "raw" data enter at the top, and the useful representations of the information are shown at the bottom as the products of the analysis.

where r, θ, φ is the field point and r_0 is the reference radius taken to be the planet's mean radius. The spatial wavelength corresponding to harmonics of degree n is $\lambda = 2\pi r_0/n$. For large n and for an altitude h, low compared to r_0,

$$(r/r_0)^{-(n+2)} \approx e^{-(n+2)h/r_0} \approx e^{-2\pi h/\lambda} \quad (2)$$

The same result is easily obtained in the "flat planet" approximation. (For example, see *Goldberg and Reasenberg* [1985].)

For the PVO analysis the available resolution varies substantially over the planet's surface, principally as a function of latitude. The best resolution is at the latitude of periapsis: $h_{\min} \geq 140$ km; $2\pi(140\text{ km}) = 8.2°$ on the surface. To model the gravity at this resolution over the entire surface would require about 2.6×10^3 parameters, independent of the (nonredundant) form chosen for the gravity representation. Further, because of the variability of h, such a large number of parameters could not be independently determined. An attempt to do so would result in a degenerate (i.e., severely ill-conditioned) estimator.

Taking the apparently conservative approach of estimating a model of uniformly low resolution is not an entirely satisfactory solution for two reasons. First, such a model would fail to represent all of the available information. Second, the unmodeled, high-spatial-frequency signatures in the gravity would be aliased into the modeled, lower-frequency signatures. Thus we are forced to the conclusion that the ideal representation would permit the resolution of the model to be variable over the planet surface such that it could reflect the intrinsic resolution of the data.

The motions of Earth and Venus cause the observing geometry to vary with time. (Precession of the spacecraft orbit is relatively slow.) An analysis technique that requires a special observing geometry will, at best, be applicable to a small fraction of the available data and therefore should not be considered. However, even the most robust estimators show a decreased information rate for certain unfavorable geometry including an Earth-Sun-Venus angle near 180°.

The classical approach of the celestial mechanician is to expand the central body potential as a spherical harmonic series and to analytically determine the effects of the individual terms of the series on the spacecraft orbital elements. The spacecraft orbit would then be determined from each of several short spans of data and the evolution of the elements used to estimate the harmonic series coefficients. For the ab initio analysis of the PVO tracking data, this approach has two fatal flaws. First, the spherical harmonic representation yields a uniform surface resolution which, as previously discussed, is inappropriate to the PVO problem. Second, the use of orbital elements discards too much of the information content of the data.

A Venus gravity model was determined by *Ananda et al.* [1980] from the analysis of the evolving spacecraft orbital elements. A principal motivation for this work was the availability of the spacecraft elements as determined each day by the PVO Navigation Team. The cost of the final analysis was thus relatively low, making this an attractive type of study. However, the model is of low resolution.

Early planetary and lunar orbiter gravity analyses included the direct, least squares estimation of harmonic coefficients from the Doppler tracking data. (Attempts to use ranging data were generally not successful.) It was widely believed that the best results would be obtained from the analysis of the longest possible continuous spans of data. This belief appears to have been based on an examination of the variational equations which showed increased sensitivity with time.

In determining the gravity field of Mars from the Mariner 9 tracking data, *Reasenberg et al.* [1975, p. 89] showed that the direct, least squares analysis yielded better (i.e., more consistent) results when the data spans were broken, even though this required increasing the parameter set to include additional sets of spacecraft elements. The work was motivated by a concern for the effects "of important random, or quasi-random, accelerations of the spacecraft, due, for example, to imbalances in the gas jets used to control the orientation of the spacecraft . . ." The multiple short-arc analysis was viewed as an approximation to a Kalman filter which, at the time, had neither been implemented in our software, nor used by any group to estimate planetary (or lunar) gravity.

For a Venus gravity model based on the PVO tracking data and spherical harmonics, the previously discussed conflict over resolution would be particularly severe. A possible solution to this conflict would be to introduce a priori constraints on the estimated parameters such that the effective resolution would vary over the surface in correspondence to the intrinsic resolution of the data. Although this is possible in principle, we know of no case in which this approach has been applied to the determination of a gravity model. Even if it were to be applied, in the case of PVO, it would result in the need for computationally burdensome data processing. In the absence of such a constraint, the model would likely contain artifacts not usefully related to the actual gravity of the planet. For example, these might appear as features of small lateral extent in a region where the data are unable to support such resolution, i.e., away from the periapsis latitude. The alternative of using a diagonal a priori constraint yields an undesirable bias to all harmonic coefficients.

The earliest use of short-arc analysis was by *Muller and Sjogren* [1968]. They mapped the Doppler residual rate directly to the surface of the Moon along the line of sight. This direct residual mapping (DRM) technique permitted them to make the first detection of the lunar mascons. DRM has been used extensively by W. L. Sjogren and his coworkers [e.g., *Sjogren et al.*, 1974, and references therein]. The technique has proved of great value for a first, qualitative examination of gravity, since it yields maps of good resolution with a minimum of data processing. However, because there is no inversion involved, the resulting gravity maps are ill-suited for direct quantitative interpretation as noted (often and with clarity) by Sjogren, who cites numerical studies by *Gottlieb* [1970].

Of course, in the same way one could use the Doppler data, it is possible to use a DRM to fit a specific geophysical model, as was done by *Phillips et al.* [1978]. Thus one might be persuaded that all gravity representations are equally good since to correctly test a specific geophysical model requires calculating the corresponding external gravity map that would have been determined by the method used for the available gravity model. However, an inversion which maintains the full resolution of which the data are capable provides better discrimination among geophysical models; a clean inversion better supports the synthesis of useful hypotheses and their preliminary testing.

Over the years, several ad hoc schemes for inverting Doppler gravity data have been proposed. (For example, see *Bowin* [1983]. In his Figure 9 the two sets of discontinuities, which follow spacecraft tracks and are each due to a transition from one set of contiguous tracks to another, attest to the failure of the technique.) Such schemes may yield maps that give the appearance of being sensible but which can make no contribution to the knowledge of the internal structure of the body. (To the extent that they are used for further analysis, such maps may interfere with progress.) This is particularly regretable since the literature contains numerous good papers on the geophysical inverse problem including *Backus and Gilbert* [1970], *Burkhard and Jackson* [1976], *Moritz* [1976, 1978], and *Jackson* [1979].

If the ad hoc schemes are incorrect, why do the maps look plausible? An inversion is generally a linear operation on the data to yield a gravity map. The Doppler tracking data are "closely related" to the gravity as evidenced by the success of the DRM. A plausibly useful linear operation on a DRM would result in location-dependent shifts in the amplitude and phase of the components of the map but would not be likely to obscure or reveal major features. The same is true of a linear operation on the Doppler residuals. It is hard to imagine an inversion technique being proposed and found to obscure the major features of the gravity field. However, there is a considerable difference between not obscuring features and yielding a map suited to quantitative interpretation. The former is hardly an achievement; the latter was the objective of our analysis.

4. The Kalman Filter in PEP

The Kalman filter (KF) in PEP has a few unusual features. These and some other pertinent aspects are described here functionally; the details of the implementation are driven by the peculiarities of PEP. In section 5, we present the results of several numerical tests of the PEP KF.

In the classical KF, the state estimate is updated with each datum. The state estimate and covariance are propagated forward, and the effect of the process noise is included in preparation for the next datum. In this way, the optimal estimates are available shortly after the receipt of each datum, a considerable advantage for real-time analysis and control. (For a recent astronomical application of a real-time filter, see *Reasenberg* [1990].) However, for the analysis of scientific data, immediacy is not important. Therefore, in the PEP KF, the data are collected into batches and each batch is used to form a set of normal equations as would be done for a weighted-least-squares analysis. If these normal equations were added together directly, we could obtain the standard weighted-least-squares solution.

The batch normal equations are processed in place of individual data in the PEP KF. The state is defined such that the nominal state propagation matrix is the identity. Thus, instead of including the position and velocity of a spacecraft in the state, the corresponding initial conditions are included. Since the process noise covariance is defined in terms of the spacecraft position and velocity as discussed below, the scheme requires that a set of variational equations be integrated and that these be used to map the process noise to the initial epoch. (In the more common form of the KF, those same variational equations would be required to calculate the state transition matrix.)

In the PEP KF analysis of the PVO tracking data, we have an advantage not usual in the KF analysis. The PVO Navigation Team used single-day batches of data to determine the spacecraft state for most of the first 600 days of the orbital phase of the mission. Although these state estimates were found to differ slightly from those derived by PEP, as initial estimates, they proved indispensable to the efficient conduct of our analysis. The PEP KF contains a provision to accept initial state estimates at several epochs during the time span under consideration. In the first step of the analysis, these are used to find a reference trajectory. Starting with the earliest epoch, the trajectory is numerically integrated until the next epoch. Here an integration transition is performed: The difference between the integrated and externally supplied states is found and mapped to the initial epoch using the variational equations. The current state difference is used to modify the difference tables of the numerical integration so that the trajectory passes through the new externally supplied point and continues. The state offset is mapped to the initial epoch and saved to be used with the linearized estimator. This process is repeated for each of the state vectors until the requested end of the integration is reached.

The atmospheric drag at periapsis makes the PVO trajectory analysis significantly less linear than the corresponding drag-free problem. In our early analyses, before the implementation of the multistate starting procedure, the trajectory fitting typically required six iterations per batch of data. With the multistate starting procedure, the initial (segmented) trajectory proved to be so close to "correct" that no iteration was necessary as will be discussed in the next section. Doppler residuals, suitable for geophysical inversion, were obtained by linear prediction from the prefit residuals, the state adjustment vectors of the first KF solution, and the sensitivity matrix (i.e., $\partial z/\partial \alpha$, where z is the observable and α is the vector of parameters).

The process noise model consisted of two parts. The first applied to the atmospheric density parameter and was made large enough that the density estimates for adjacent days were essentially independent. The second part of the model was an isotropic acceleration variance density. Each Cartesian component had an amplitude of 10^{-19} AU^2/d^3.

5. Kalman Filter Performance

We have conducted two types of tests of the PEP KF as used for the analysis of the PVO Doppler data. In the first set of tests, we used Doppler residuals kindly provided to us by W. L. Sjogren of the Jet Propulsion Laboratory (JPL). We compared these to the corresponding PEP KF residuals. In the second set of tests, PEP was used to numerically integrate a PVO trajectory with one of several models and to calculate the expected Doppler data. The PEP KF was used to analyze these simulated data and the resulting postfit residuals, or derived Doppler rate residuals, were investigated. Below we discuss the two sets of tests.

JPL Comparison

Sjogren provided us with residuals that he had obtained from his own (PVO) spacecraft orbit determinations. In this work, he used 2-hour spans of tracking data starting 1 hour before periapsis and ending 1 hour after periapsis. The

trajectory was integrated using an atmospheric model determined for each orbit by the Navigation Team.

A comparison of the Doppler residuals showed a systematic difference that is no larger than the data noise. This difference has no apparent high-frequency component and thus no effect on the gravity model. (Note that the data noise cancels in this comparison.) We concluded that there would be little difference in our maps were we to replace our KF residuals with Sjogren's short-arc batch-analysis residuals.

Simulation Study

We have done a series of numerical experiments that address the accuracy of the PEP KF analysis of the PVO data. In each experiment, PEP was used first to integrate a spacecraft trajectory with a given set of parameters and second to calculate the corresponding Doppler observables. The PEP KF was used to estimate a "best fit" filter trajectory assuming no anomalous gravity and a nominal atmospheric scale height. The resulting Doppler residuals were numerically differentiated to determine the Doppler rate residuals, which were expected to be proportional to the "line-of-sight" (LOS) component of the unmodeled part of the spacecraft acceleration.

In each study discussed below, we simulated the same set of seven contiguous orbits (beginning and ending at apoapse), with initial conditions (IC) and epoch taken from an actual PVO orbit. The times and IC for each KF epoch were obtained from the simulations, with IC rounded to from 7 to 10 figures, to mimic the typical accuracy of the (JPL) IC used in actual PVO/KF orbit determinations (OD). In actual OD, perturbations due to solar gravitation and solar radiation are modeled. In both the simulations and the OD for the numerical studies, the former perturbation is included, the latter is not. Planetary perturbations of the spacecraft, which are not included in the analyses of the PVO tracking data, were not included in the simulations.

In the first numerical experiment, the initial integration assumed neither atmospheric drag nor anomalous gravity. Thus the KF deterministic model was correct. The resulting LOS residuals were systematic (presumably due to imperfect adjustment of the rounded IC) and had a RMS of under 0.0003 mGal and a peak of 0.0012 mGal in the periapsis region. This is about 4 orders of magnitude below either the typical error due to the inversion or the worst errors encountered in the other KF tests.

In the second numerical experiment, the initial integration model included three gravity-harmonic terms ($J_3 = 5 \times 10^{-5}$, $J_{10} = -3 \times 10^{-5}$, $C_{20,5} = 1 \times 10^{-5}$) and zero atmospheric density. The LOS residual is shown in Figure 3*a* along with the difference between this and the expected LOS acceleration calculated directly from the gravity-harmonic terms. This difference, which is on a 10X finer scale, does not appear to include the signature of the gravity model; the resulting error is presumed to be under 1%.

In the third numerical experiment, the gravity-harmonic terms were zero but atmospheric drag was included in the initial integration. The atmospheric density ρ at altitude z was modeled as

$$\rho(z) = \rho_0 e^{-(z-z_0)/H} \tag{3}$$

where ρ_0 is the density at the reference altitude z_0 and H is the scale height. For the integration we used $H = 7$ km, $z_0 = 150$ km, and $\rho_0 = 5 \times 10^{-13}$ g/cm^3. In the KF analysis, we used a scale height of $H' = 10$ km and the previous value for z_0. We selected ρ_0 such that for the first periapsis passage, $\rho(z_p)$, the density at periapsis, yielded about the correct value of $\rho_p H^{1/2}$, since this value would tend to keep the problem from becoming excessively nonlinear. (A similar approach was used with the real data; the value of $\rho(z_p)H^{1/2}$ was obtained from the orbital elements determined by the JPL Navigation Team.)

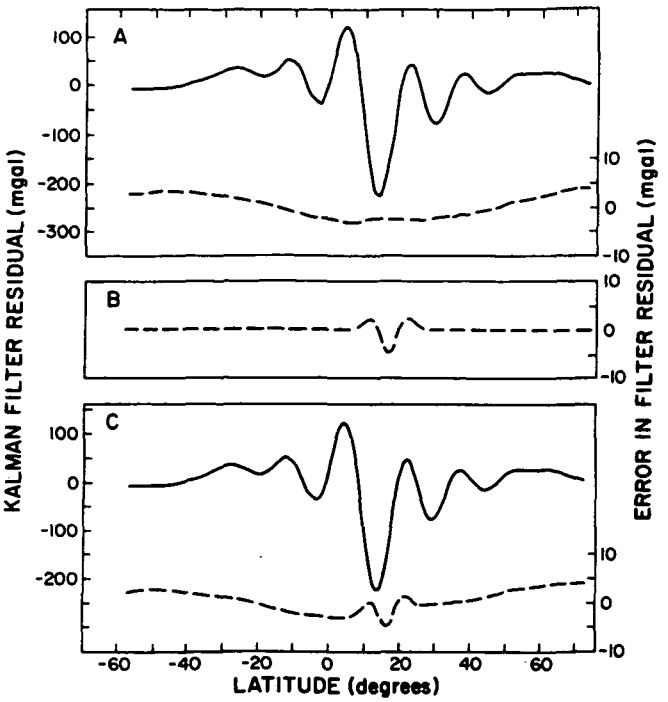

Fig. 3. Results of tests of the performance of the Kalman filter (KF). These test address the question: To what extent does the filter yield the line-of-sight (LOS) acceleration of the spacecraft? See text for a description of the tests. Solid curve shows LOS residual; dashed curve shows difference between LOS residual and expected acceleration due to gravity harmonics. (*a*) Experiment two, recovery of gravity harmonics. (*b*) Experiment three, effect of atmospheric drag. (*c*) Experiment four, combination of gravity harmonics and atmospheric drag.

Figure 3*b* shows the LOS residual from the KF fit. The signature is that expected from the use of a "wrong" scale height in the KF. Table 1 (experiment 3) shows the determination of the atmospheric density by the KF. It is easily shown that the change of spacecraft orbital period due to drag is proportional to $y = \rho(z_p)H^{1/2}$. Table 1 shows that this quantity is estimated with a small fractional error although the error is large compared to the standard deviation σ. Based on the analysis of the PVO data, we know that the density shows much larger fluctuations.

The mismatch in scale height used in this test is larger than we expect most of the corresponding mismatches to be in the actual data analysis. Further, in the geophysical inversion, information from several spacecraft passes is combined (averaged) to produce the gravity estimate. Thus unless the scale height is systematically incorrect for several days, there should be some reduction of the effect of the atmosphere mismodeling on the gravity model. We therefore expect the atmospheric modeling errors to result in gravity model errors of well under 5 mGal.

TABLE 1. Determination of Atmospheric Density by the Kalman Filter

Orbit	$z_p - z_0$, km	$\hat{z}_p - z_0$, km	$\hat{\rho}_0$, 10^{-13} g/cm^3	$\rho(z_p)$, 10^{-13} g/cm^3	$\hat{\rho}(\hat{z}_p)$, 10^{-13} g/cm^3	$y = \frac{\rho(z_p)}{H^{1/2}}$	$\hat{y} - y$	σ	$(\hat{y} - y)/\sigma$
				Experiment 3					
1	0.15	0.15	4.12	4.89	4.06	12.9	−0.114	0.0064	−18
2	0.79	0.79	4.01	4.46	3.71	11.8	−0.090	0.0063	−14
3	1.57	1.57	3.87	4.00	3.31	10.6	−0.117	0.0062	−19
4	2.48	2.47	3.71	3.51	2.90	9.3	−0.117	0.0060	−20
5	3.53	3.53	3.53	3.02	2.48	8.0	−0.148	0.0059	−25
6	4.72	4.72	3.37	2.55	2.10	6.7	−0.100	0.0059	−17
7	6.06	6.06	3.17	2.10	1.73	5.6	−0.106	0.0060	−18
				Experiment 4					
1	0.25	0.27	4.31	4.82	4.19	12.8	0.502	0.0065	78
2	1.01	1.05	4.20	4.33	3.79	11.4	0.527	0.0063	84
3	1.91	1.96	4.06	3.81	3.34	10.1	0.478	0.0062	77
4	2.94	2.98	3.87	3.28	2.88	8.7	0.407	0.0060	68
5	4.12	4.14	3.71	2.78	2.45	7.3	0.398	0.0060	67
6	5.43	5.45	3.55	2.30	2.06	6.1	0.412	0.0059	70
7	6.89	6.93	3.40	1.87	1.70	4.9	0.432	0.0060	72

The model of the atmospheric density ρ and its parameters $\rho_0 = 5 \times 10^{-13}$ g/cm^3, $z_0 = 150$ km, and $H = 7$ km, are defined in the text. The variables with a circumflex (e.g., $\hat{\rho}$) refer to quantities estimated (directly or indirectly) in the KF orbit determination; the corresponding unmarked variables refer to their "true" values, i.e, those used in or obtained from the original simulation. z_p is the spacecraft altitude at periapse, y is the quantity proportional to the change in orbital period, $H = 7$ km and $H' = 10$ km are the scale heights used in the simulation and KF, respectively, and σ is the formal error for $\hat{y}$.

In the fourth numerical experiment, the initial integration combined the gravity model of experiment 2 with the atmospheric model of experiment 3. The KF again used the "wrong" scale height, $H' = 10$ km. Figure 3*c* shows the LOS residual and, again on a 10X finer scale, the difference between this residual and the expected contribution due to the harmonics. Table 1 (experiment 4) shows the density determination by the KF. Although the errors in the density estimates (see $\hat{y}$-y in Table 1) are 3–6 times those of the previous case, they are still small compared to the day-to-day fluctuations seen in the PVO-derived density estimates. Thus it is better to estimate ρ for each periapsis pass than to assume ρ_0 constant, even for a few days.

A comparison of the error in the KF accelerations of Figure 3*c* with those of Figures 3*a* and 3*b* shows that the error produced by a combination of unmodeled anomalous gravity and incorrectly modeled atmospheric density is, to a good approximation, simply the sum of the errors due to each model error individually. This, as well as the results presented in Table 1, indicates that the low-frequency gravitational harmonics are not significantly "absorbed" or "aliased" as atmospheric process noise.

We extended the above numerical experiments to examine the errors introduced by not iterating the estimator. In the iteration associated with experiment 2 (gravity harmonic terms but no atmospheric drag), the estimator required two iterations to converge plus one to confirm convergence. We found in experiment 3 (drag but no harmonics) that, as suggested by previous work, the atmospheric drag term made the problem highly nonlinear. (This reflects the small scale height of the atmosphere.) The same nonlinearity was present when the gravity harmonic terms were added (experiment 4); the gravity terms caused larger adjustments to the elements and thus tended to hide the nonlinearity. The iteration showed

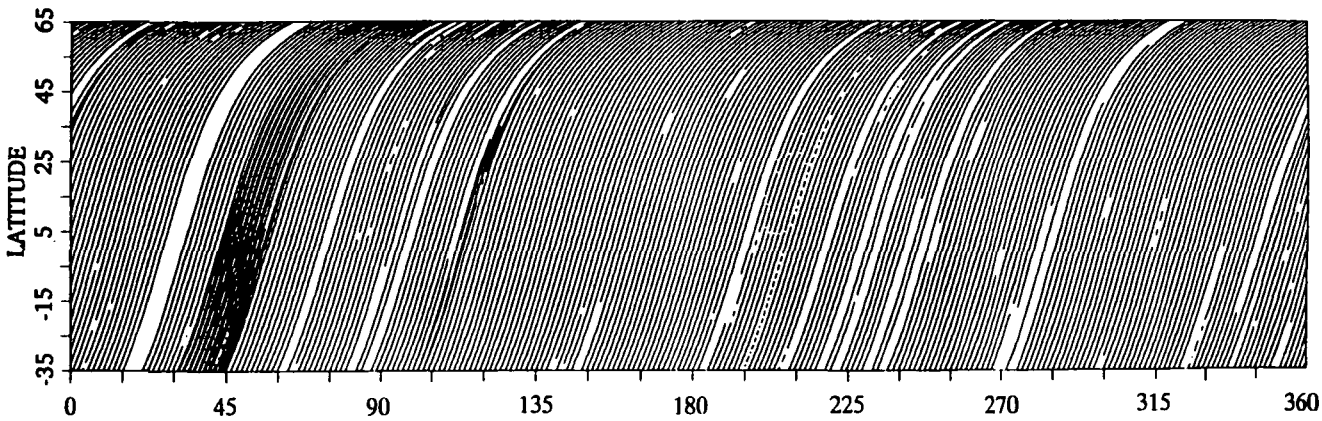

Fig. 4. Spacecraft tracks projected on the surface of Venus and shown 5° past the upper and lower edges of the maps in the color plate. For the gravity inversion, data were used from somewhat beyond the region shown here: in particular, we excluded all data taken with a spacecraft altitude of more than 4000 km.

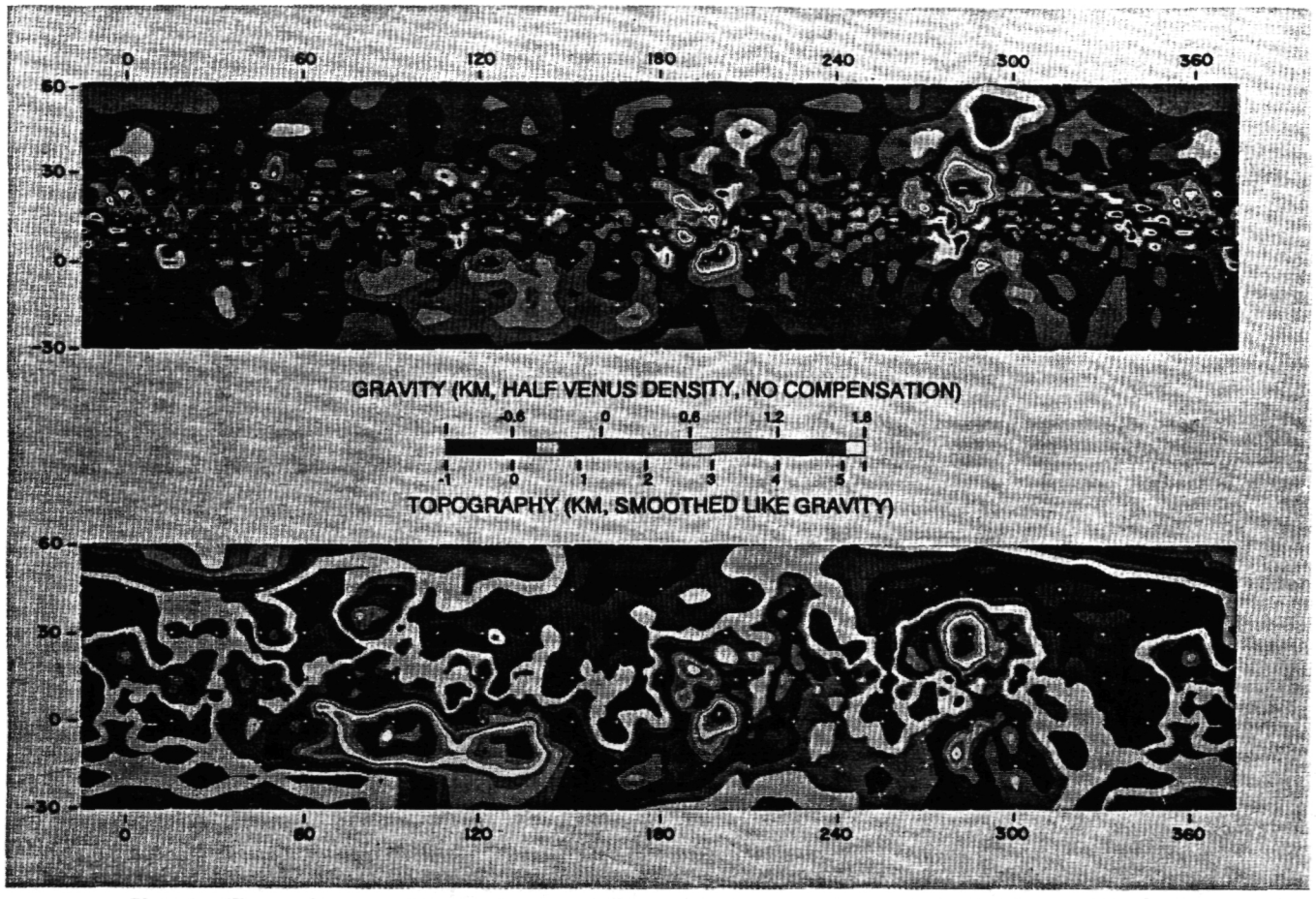

Plate 1. The gravity map (above) and corresponding smoothed topography map (below) of Venus. These maps cover 2/3 of the surface of Venus and are cut off where the resolution has become poor. The false color of the maps correspond to altitude. For the gravity map, it is the altitude to which material of density half the mean density of Venus would need to be piled to yield the observed external potential. The color bar between the maps shows increasing altitude from left to right in steps of 150 m and 333 m for the gravity and topography maps, respectively. Near periapse, the discretization limits the resolution of the gravity map to $\lambda = 4°$. However, the combination of the exponential loss of signal (equation (2)) and the behavior of the estimator cause the response to roll off as the wavelength gets small. We estimate the effective resolution to be $\lambda = 6°$ at periapsis and to be larger by a factor of 10 at the upper and lower edges of the map. By construction, the topography map should have the same resolution characteristics (and the same distortions) as the gravity map.

that the Doppler rate residuals from the converged solution differed systematically from the ones predicted linearly from the first iteration by about 0.2 mGal RMS; no damage is done to our gravity maps by not iterating.

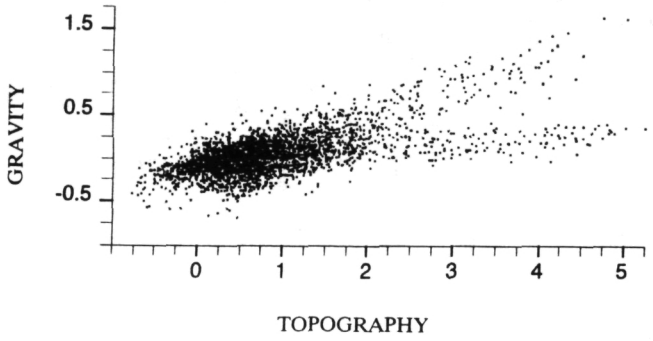

Fig. 5. Scatter of gravity (vertical axis) versus topography, from the same data displayed in Plate 1, taken in the band of highest resolution, between 5°S and 35°N over the full longitude range at 1° lattice points. The units for the respective quantities are the same as in Plate 1.

6. Data Analysis and Results

Plate 1 shows false-color images of our gravity map (top) and the corresponding smoothed topography map (bottom). These have been scaled to provide easy comparison. The maps are based on the combined results of nine separate inversions, and incorporate 1.2×10^5 Doppler rate data from 251 spacecraft revolutions, which occurred between April 1979 and August 1980. Displayed in Figure 4 are projections on the Venus surface of the spacecraft trajectory at the transpond times of the Doppler data we used. Note that the gravity map shows no evidence of either the data gaps or the redundancy near 45°E longitude. The orbits were determined in 38 separate Kalman filter batches, generally comprising six to eight orbital revolutions each. The breaks between batches were usually dictated by the occurrence of propulsive spacecraft maneuvers.

We model the external gravity as the sum of a point mass centered on the planet and a surface mass density. In each inversion region, we have discretized the planetary surface with lines of constant latitude or longitude. This gives rise to trapezoidal cells (neglecting curvature), which we take to

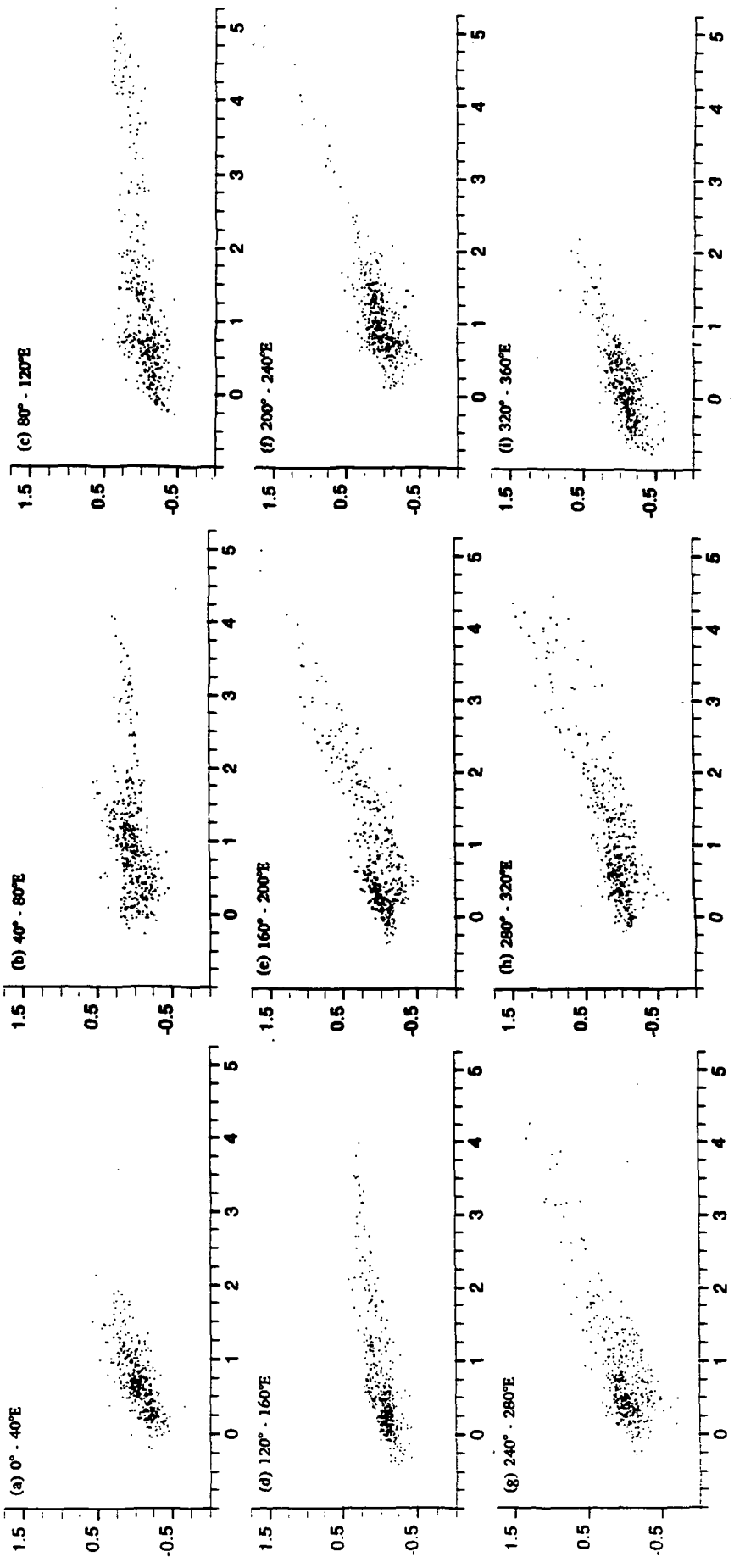

Fig. 6. Scatter plots of gravity and topography, as in Figure 5, but from 40° × 40° regions; (*a*) 0°–40°E; (*b*) 40°–80°E; (*c*) 80°–120°E; (*d*) 120°–160°E; (*e*) 160°–200°E; (*f*) 200°–240°E; (*g*) 240°–280°E; (*h*) 280°–320°E; (*i*) 320°–360°E.

have uniform surface mass densities. At periapsis, the cells are 2° × 2°, and for the highly eccentric orbit of PVO, we advantageously make the linear dimension of each cell roughly proportional to the local spacecraft altitude. The cell is divided into four (i.e., 2 × 2) "subcells," and the field of each subcell is modeled as the sum of a centered point mass and quadrupole; the dipole term is neglected.

As discussed by *Goldberg and Reasenberg* [1985], the data inversion is performed by a linear Bayesian least squares estimator in which we use the weighted Jekeli covariance to form an a priori covariance matrix. We set a 500-parameter limit to the inversions, which permits a region covering about 60° of longitude. We established inversion regions that have a considerable overlap. Within each overlapping portion is a strip in which there is not a significant difference between the two adjacent inversion regions. The data displayed at each point in the maps of Plate 1 either are taken directly from a single inversion region or are the weighted average of the data from two regions within such a strip of near agreement. In the latter case, the weighting varies linearly across the strip.

A cursory examination of Plate 1 reveals what has long been known, that gravity is well correlated with topography at long spatial wavelengths. More careful examination reveals that this correlation continues down to the smallest wavelengths resolved: virtually every visible feature in the smoothed topographic map has a gravitational counterpart. The reverse is not always true. However, many apparently unmatched small gravitational features do have counterparts in the unsmoothed topography [e.g., *Pettengill et al.*, 1980]. For example, the principal peaks and central depression seen in the gravity over Asteria Regio (around 20°N, 265°E) all correspond to real topographic features that are not seen in the smoothed topography map. A similarly strong example can be seen in the detailed structure of Atla Regio (5°–25°N, 180°–200°E).

It appears that most gravitational features that are at least two contour levels high have a real topographic counterpart. The preferential absence of many of these counterparts from the filtered topography for short spatial wavelengths is an indication that the spectral admittance on Venus tends to be higher at shorter wavelengths than at longer ones [cf. *Goldberg and Reasenberg*, 1985]. That many single-contour-level gravitational features do not have counterparts in the topographic data is consistent with our estimate of the noise level of the gravity map which is about one contour.

It has been apparent from the low-frequency gravity studies that the level of isostatic compensation on Venus is far from uniform. In fact, the term compensation may be misdescriptive since at least some of the features may be the result of dynamic processes [*Kiefer et al.*, 1986]. Some large topographic features of unusually high elevation, such as Beta Regio (25°N, 280°E) and Ulfram Regio (5°N, 200°E), correspond to similarly extreme gravitational features, while other high topographic regions, such as those in western Aphrodite Terra (5°S, 85°E and 10°S, 135°E), correspond to relatively modest gravity peaks. In Plate 1, such contrasts can also be seen for much smaller features, such as the components of Phoebe Regio (0°–20°S, 275°–300°E), Eisila Regio (10°–30°N, 10°W–30°E), and the region west of Beta Regio (0°–45°N, 210°–260°E).

There appear to be two distinct trends of isostatic compensation, as evidenced by the bifurcated relation between gravity and topography as seen in Figure 5. In the units of our maps, one trend in this scatter plot has a gravity-to-topography ratio of about 1/3; the other, about 1/10. This bimodality occurs locally as well as planet wide. Figure 6 shows the slopes of 1/3 and 1/10 appearing in smaller regions, with little or no evidence for other slopes. Of particular interest is the appearance of the 1/3 slope in Figures 6*a* and 6*b*, where it occurs in regions between 0 and 2 km elevation. Such "rolling plains" regions have been thought to be more fully compensated than other portions of the planet, but this appears not always to be the case.

7. Summary

We have developed techniques that permit the efficient and accurate determination of the gravity field of a planet from the Doppler tracking of an orbiting spacecraft. These techniques work in the case of a highly eccentric orbiter and permit a gravity model whose resolution varies over the surface of the planet as required, for example, corresponding to the local spacecraft altitude.

We have applied these techniques to the Doppler tracking data from the Pioneer Venus Orbiter to yield a Venus gravity model. The gravity map appears devoid of the computational artifacts that have traditionally plagued planetary gravity inversions. In particular, all of the features of the gravity map that are larger than the noise level correspond to topographic features. Since no topographic information was used in the inversion of the Doppler data to yield the gravity map, the strong correspondence is taken to be real and to indicate a lack of artifacts. (The conspiracy theory is rejected.)

In order to permit an easy comparison of the gravity and topography, we have generated a topography map with the same resolution and distortion as the gravity map. This smoothed topography map was made by (1) converting the high-resolution topographic data from the PVO altimeter into pseudo-Doppler data that correspond to the real Doppler data and (2) performing the same inversion on these as on the real Doppler data. Scatter plots of gravity against smoothed topography show two distinct trends, suggesting two modes of topographic support or history. More detailed analysis of this phenomenon, for example by means of spectral admittance, seems warranted.

Note that the digital data that were used to make the two maps in Plate 1 have been provided to the Magellan Project for their preencounter data set and to the NSSDC for distribution.

Acknowledgments. We are grateful for the aid of the PVO Navigation Team who provided us with the spacecraft tracking data, orbital element estimates, and other useful information. We thank W. L. Sjogren for helpful discussions. We are indebted to E. Eliason and the late H. Masursky of the US Geological Survey for the preparation of the colored maps of gravity and topography from our grid arrays. This work was supported in part by NASA Research grants NAGW-409, NAGW-1438, and NAGW-2361 and by the Smithsonian Institution, both directly and through its Scholarly Studies Program, which provided support for computing.

References

Akim, E. L., Z. P. Vlasova, and I. V. Chuik, Determination of the dynamic compression of Venus from the measured trajectories of

its first artificial satellites, Venera 9 and Venera 10, *Dokl. Akad. Nauk SSSR, 240*, 556–559, 1978.

Ananda, M. P., W. L. Sjogren, R. J. Phillips, R. N. Wimberly, and B. G. Bills, A low-order gravity field of Venus and dynamical implications, *J. Geophys. Res., 85*, 8303–8318, 1980.

Anderson, J. D., and L. Efron, The mass and dynamical oblateness of Venus, *Bull. Am. Astron. Soc., 1*, 231, 1969.

Ash, M. E., Determination of Earth satellite orbits, *Tech. Note 1972-5*, MIT Lincoln Lab., Lexington, Ky., 1972.

Backus, G., and F. Gilbert, Uniqueness in the inversion of inaccurate gross earth data. *Philos. Trans. R. Soc. London, Ser. A, 266A*, 123–192, 1970.

Bills, B. G., W. S. Kiefer, and R. L. Jones, Venus gravity: A harmonic analysis, *J. Geophys. Res., 92*, 10,335–10,351, 1987.

Bowin, C., Gravity, topography and crustal evolution of Venus, *Icarus, 56*, 345, 1983.

Burkhard, N., and D. D. Jackson, Application of stabilized linear inverse theory to gravity data, *J. Geophys. Res., 81*, 1513–1518, 1976.

Colin, L., The Pioneer Venus program, *J. Geophys. Res., 85*, 7575–7598, 1980.

Gelb, A. (Ed.), *Applied Optimal Control*, MIT Press, Cambridge, Mass., 1974.

Goldberg, Z. M., and R. D. Reasenberg, Venus gravity west of Beta Regio, *Icarus, 62*, 129–142, 1985.

Gottlieb, P., Estimation of local lunar gravity features, *Radio Sci., 5*, 301–312, 1970.

Howard, H. T., et al., Venus: Mass, gravity field, atmosphere, and ionosphere as measured by the Mariner 10 dual-frequency radio system, *Science, 183*, 1297–1301, 1974.

Hunten, D. M., L. Colin, T. M. Donahue, and V. I. Moroz (Eds.), *Venus*, University of Arizona Press, Tucson, 1983.

Jackson, D. D., The use of a priori data to resolve non-uniqueness in linear inversion, *Geophys. J. R. Astron. Soc., 57*, 137–157, 1979.

Jazwinski, A. H., *Stochastic Processes and Filtering Theory*, Academic, San Diego, Calif., 1970.

Kiefer, W. S., M. A. Richards, B. H. Hager, and B. G. Bills, A dynamic model of Venus's gravity field, *Geophys. Res. Lett., 13*, 14–17, 1986.

Lewis, B. T. R., and L. M. Dorman, Experimental isostasy, 2, An isostatic model for the United States derived from gravity and topographic data, *J. Geophys. Res., 75*, 3367–3386, 1970.

McKenzie, D., and C. Bowin, The relationship between bathymetry and gravity in the Atlantic Ocean, *J. Geophys. Res., 81*, 1903–1915, 1976.

McNutt, M., Implications of regional gravity for state of stress in the Earth's crust and upper mantle, *J. Geophys. Res., 85*, 6377–6396, 1980.

Moritz, H., Least-squares collocation as a gravitational inverse problem, *Rep. 249*, Dep. of Geod. Sci., Ohio State Univ., Columbus, 1976.

Moritz, H., Least squares collocation, *Rev. Geophys., 16*, 421–430, 1978.

Mottinger, N. A., W. L. Sjogren, and B. G. Bills, Venus gravity: A harmonic analysis and geophysical implications, *Proc. Lunar Planet. Sci. Conf. 15th*, Part 2, *J. Geophys. Res., 90*, suppl., C739–C756, 1985. (Correction, *J. Geophys. Res., 90*, suppl., D197–D200, 1985.)

Muller, P. M., and W. L. Sjogren, Mascons: Lunar mass concentrations, *Science, 161*, 680–684, 1968.

Pettengill, G. H., E. Eliason, P. G. Ford, G. B. Loriot, H. Masursky, and G. E. McGill, Pioneer Venus radar results: Altimetry and surface properties, *J. Geophys. Res., 85*, 8261–8270, 1980.

Phillips, R. J., W. L. Sjogren, E. A. Abbott, and S. H. Zisk, Simulation gravity modeling to spacecraft-tracking data: Analysis and application, *J. Geophys. Res., 83*, 5455–5464, 1978.

Phillips, R. J., W. L. Sjogren, E. A. Abbott, J. C. Smith, R. N. Wimberly, and C. A. Wagner, Gravity field of Venus: A preliminary analysis, *Science, 205*, 93–96, 1979.

Reasenberg, R. D., Kalman-filter fringe tracking in an optical interferometer, in *Proceedings of SPIE's 1990 Symposium on Astronomical Telescopes and Instrumentation for the 21st Century, Amplitude and Intensity Spatial Interferometry*, edited by J. B. Breckinridge, Paper 1237, pp. 172–182, Society of Photo-Optical Instrumentation Engineers, Bellingham, Wash., 1990.

Reasenberg, R. D., I. I. Shapiro, and R. D. White, The gravity field of Mars, *Geophys. Res. Lett., 2*, 89–92, 1975.

Reasenberg, R. D., Z. M. Goldberg, P. E. MacNeil, and I. I. Shapiro, Venus gravity: A high resolution map, *J. Geophys. Res., 86*, 7173–7179, 1981.

Reasenberg, R. D., Z. M. Goldberg, and I. I. Shapiro, Venus: Comparison of gravity and topography in the vicinity of Beta Regio, *Geophys. Res. Lett., 9*, 637–640, 1982.

Sjogren, W. L., R. N. Wimberly, and W. R. Wollenhaupt, Lunar gravity via the Apollo 15 and 16 subsatellites, *Moon, 9*, 115–128, 1974.

Sjogren, W. L., R. J. Phillips, P. W. Birkeland, and R. N. Wimberly, Gravity anomalies on Venus, *J. Geophys. Res., 85*, 8295–8302, 1980.

Sjogren, W. L., B. G. Bills, P. W. Birkeland, P. B. Esposito, A. R. Konopliv, N. A. Mottinger, S. J. Ritke, and R. J. Phillips, Venus gravity anomalies and their correlations with topography, *J. Geophys. Res., 88*, 1119–1128, 1983.

Sjogren, W. L., B. G. Bills, and N. A. Mottinger, Venus: Ishtar gravity anomaly, *Geophys. Res. Lett., 11*, 489–491, 1984.

Williams, B. G., N. A. Mottinger, and N. D. Panagiotacopulos, Venus gravity field: Pioneer Venus orbiter navigation results, *Icarus, 56*, 578–589, 1983.

Z. M. Goldberg and R. D. Reasenberg, Harvard Smithsonian Center for Astrophysics, 60 Garden Street, Cambridge, MA 02138.

(Received October 23, 1990;
revised June 26, 1992;
accepted June 26, 1992.)